The Astrophysical Journal, 656: L101–L104, 2007 February 20

CORONAL "WAVE": MAGNETIC FOOTPRINT OF A CORONAL MASS EJECTION?

Gemma D. R. Attrill,[1] Louise K. Harra,[1] Lidia van Driel-Gesztelyi,[1,2,3] and Pascal Démoulin[2]
Received 2006 October 13; accepted 2007 January 18; published 2007 January 31

ABSTRACT

We investigate the properties of two "classical" EUV Imaging Telescope (EIT) coronal waves. The two source regions of the associated coronal mass ejections (CMEs) possess opposite helicities, and the coronal waves display rotations in opposite senses. We observe deep core dimmings near the flare site and also widespread diffuse dimming, accompanying the expansion of the EIT wave. We also report a new property of these EIT waves, namely, that they display dual brightenings: persistent ones at the outermost edge of the core dimming regions and simultaneously diffuse brightenings constituting the leading edge of the coronal wave, surrounding the expanding diffuse dimmings. We show that such behavior is consistent with a diffuse EIT wave being the magnetic footprint of a CME. We propose a new mechanism where driven magnetic reconnections between the skirt of the expanding CME magnetic field and quiet-Sun magnetic loops generate the observed bright diffuse front. The dual brightenings and the widespread diffuse dimming are identified as innate characteristics of this process.

Subject headings: Sun: activity — Sun: coronal mass ejections (CMEs) — Sun: filaments — Sun: magnetic fields

1. INTRODUCTION

The first observations of large-scale transient coronal waves were made by the *Solar and Heliospheric Observatory* (*SOHO*) EUV Imaging Telescope (EIT; Delaboudinière et al. 1995). Since the mean EIT wave speed (Klassen et al. 2000) exceeds the sound speed in the corona and the intrinsic characteristics of a fast-mode shock are capable of producing brightening in EUV images, authors such as Wang (2000), Ofman & Thompson (2002), Warmuth et al. (2004b, and references therein), and Ballai et al. (2005) endorse the interpretation of these phenomena as fast-mode waves. When EIT waves were first observed, Uchida (1968) suggested that they could be the flare-induced coronal counterpart of the hydrodynamic chromospheric Moreton fast shock wave (Moreton 1960). More recently, however, statistical studies (Biesecker et al. 2002; Cliver et al. 2005) have shown EIT waves to be more closely associated with CMEs than with flares. Chen (2006) concluded that it is unlikely that pressure pulses from flares are responsible for generating EIT waves. The interpretation of these waves as flare-induced or CME-driven thus remains open for debate.

It has also been suggested that EIT waves are not real waves at all. Rather, rearrangement of the magnetic structure during eruption of a CME may cause electric currents and pressure increases, observed as brightenings (Delannée & Aulanier 1999; Delannée 2000; Chen et al. 2002). Manoharan et al. (1996) show remote soft X-ray brightenings linked to a CME that developed into dimmings. Balasubramaniam et al. (2005) present a study of sequential chromospheric brightenings forming a large-scale propagating disturbance. Both authors speculate that the brightenings represent footpoints of overlying and nested coronal loop field lines, respectively, energized by magnetic reconnection as the fields are progressively torn away during a CME.

Since 1996, several hundred EIT waves have been observed and a picture is emerging of two distinct types of EIT wave: "S-waves" with a sharp bright front (Biesecker et al. 2002), often high velocity (greater than several hundred kilometers per second) and sometimes cospatial with a Moreton wave (Thompson et al. 2000b; Warmuth et al. 2001; Khan & Aurass 2002) and those with a more diffuse bright front (e.g., Thompson et al. 1998, 1999). By far the majority belong to the latter category (although this may be an artifact of the relatively low cadence of EIT). Harra & Sterling (2003) and Zhukov & Auchère (2004) suggest that different physical mechanisms may be responsible for the two different waves, while Thompson et al. (2000b) suggest the two types may reflect a strongly driven and then freely propagating stage of one common driver. Warmuth et al. (2004a, 2004b) and Cliver et al. (2004) argue for a unified view embracing many of the different types of large-scale solar disturbances (favoring flare- and CME-driven, respectively), including Moreton, EIT, He I 10830 Å, soft X-ray waves, and type II radio bursts.

Coronal dimming has also been associated with front-side CMEs (Thompson et al. 2000a). There appear to be two types: deep core dimmings, sometimes shown to correspond to the footpoints of the erupted flux rope (e.g., Webb et al. 2000), and a more widespread dimming, observed to correspond well to the spatial extent of CMEs detected in coronagraph data (Thompson et al. 2000a). For the well-known 1997 May 12 event, Zhukov & Auchère (2004) estimate that ~50% of the CME mass comes from the deep core dimmings and the remaining 50% from the more widespread dimmings.

In this work, we focus on the diffuse EIT coronal wave fronts and their associated dimmings. Of particular interest is the new analysis of the 1997 May 12 EIT wave by Podladchikova & Berghmans (2005), showing that the wave displays a rotation as it propagates.

2. EUV OBSERVATIONS AND DATA ANALYSIS

2.1. *Intensity Analysis of the Coronal Wave Fronts*

We present two events that possess the "classical," semi-isotropic diffuse bright front: the extensively studied event on 1997 May 12 (Thompson et al. 1998; Podladchikova & Berghmans 2005) and the event on 1997 April 7 (Thompson et al. 1999). Both events are associated with partial filament erup-

[1] University College London, Mullard Space Science Laboratory, Holmbury St. Mary, Surrey, UK; gdra@mssl.ucl.ac.uk, lkh@mssl.ucl.ac.uk, lvdg@mssl.ucl.ac.uk.
[2] Observatoire de Paris, LESIA, UMR 8109 (CNRS), Meudon-Principal Cedex, France; lidia.vandriel@obspm.fr, pascal.demoulin@obspm.fr.
[3] Konkoly Observatory, Budapest, Hungary; vandriel@konkoly.hu.

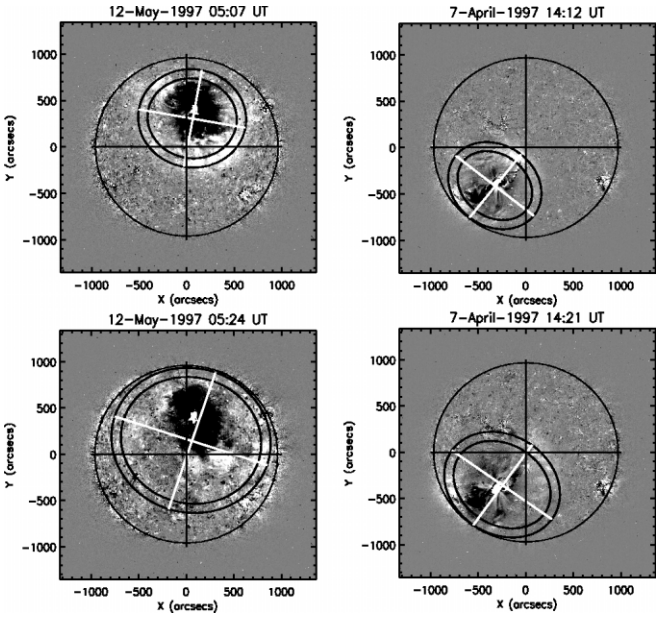

FIG. 1.—Successive base difference images for 1997 May 12 (*left*) and 1997 April 7 (*right*) coronal wave events. The bright fronts are overlaid with concentric black ellipses.

tions, flares, and front-side halo CMEs. The May event occurs in the northern hemisphere from AR 8038, which exhibits a pre-eruption reverse "S" sigmoidal structure, often cited as an indicator of negative helicity (Leamon et al. 2002). The April event is associated with AR 8027, located in the southern hemisphere, where a pre-eruption forward "S" (positive helicity) sigmoidal structure is visible.

The coronal wave of each event is captured in two successive EIT 195 Å base difference images (Fig. 1). We use running difference images to identify short-term transient features but base difference images (corrected for solar rotation) to analyze intensity, since running difference images can show false brightenings and dimmings (e.g., Chertok & Grechnev 2005). The base images are at 04:50 UT for May 12 and 14:00 UT for April 7.

After Podladchikova & Berghmans (2005), we analyze the intensity of the coronal wave front as a function of azimuthal angle around the wave front. We assume an isotropic, circular expansion around an epicenter. We account for line-of-sight (LOS) projection effects (e.g., DeForest 2004). As a result, a circular EIT wave is observed as an ellipse in projection. The ellipse characteristics are defined by the initial location of the eruption (in particular θ, the angle at the center of the solar sphere, between the observer's LOS and the initial epicenter of the eruption on the solar surface) and by the angular radius, δ, of the EIT wave (the half-cone angle subtended at the center of the solar sphere).

We sum the intensity, I, of the ring defined by the black ellipses shown in Figure 1. By changing δ and systematically shifting the center of the ellipse $\pm 10''$ about the initial epicenter (taken as the location of the associated flare: May 12, Thompson et al. 1998; April 7, Aurass et al. 2002), we objectively find the best values for the center (thus the ellipticity and the axis) and δ of the ellipse that capture most of the coronal wave intensity.

The rings defined by the black ellipses (overlaid on the bright fronts) in Figure 1 are not concentric. The projection effect implies that as the EIT wave progresses (as δ increases), the center of the projected coronal wave moves toward the disk

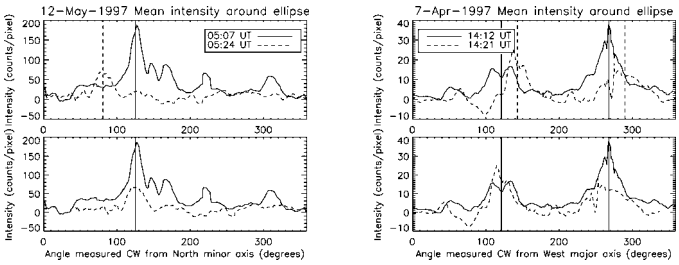

FIG. 2.—Mean intensity of the ring defined by the black ellipses shown in Fig. 1 as a function of the deprojected azimuthal angle. Left and right panels show data from the May 12 and April 7 events, respectively. The vertical lines mark the weighted mean for each peak. The lower panels show the weighted mean of the later peak(s) phase-shifted to match those of the earlier peak(s).

center. Thus, a shift of the coronal wave center is expected in the projected images, and its distance from the disk center is given by $R_\odot \sin\theta \cos\delta$.

Taking δ from the fitted black ellipses and measuring the distance from the disk center to the center of the ellipse, we compute θ for each of the ellipses. We compare this fitted θ with the θ defined by the location of the flare. The two θ's correspond relatively well, with the exception of 05:24 UT on May 12 where they differ by 10°. We attribute this difference to the distorting effect of the north polar coronal hole (Attrill et al. 2006), artificially altering the center of the ellipse and the ellipticity. The April 7 event encounters no such distortion and the two θs agree to $\pm 2°$. Thus, it is a valid assumption that the deprojected EIT waves are concentric circles, approximately centered on the flare location.

Since the projection of the wave changes as it propagates over the solar disk, using the projected azimuthal angle can induce a fake rotation. To avoid this, we plot the intensity as a function of the deprojected azimuthal angle (in the plane perpendicular to the local vertical at the epicenter of the wave, i.e., the azimuthal angle around the real circle). We use the axes of the ellipse as a reference for the azimuthal angle. The tilt of the minor axis from the main solar axes is defined solely by the epicenter of the coronal wave on the disk and therefore remains constant throughout the expansion of each event, as does the ellipticity ($=\cos\theta$).

The diffuse brightenings are highly susceptible to noise. To reduce the noise, we average the data in both the radial direction, from the inner to the outer ellipse and in the azimuthal direction, using boxcar smoothing with a smoothing kernel of 11°. The mean intensity of the ring is then plotted as a function of the deprojected azimuthal angle for the two successive images in which the coronal wave is visible (Fig. 2). The vertical lines mark the weighted mean for each peak. The lower panels show the weighted mean of the intensity of the later coronal wave front peak(s) phase-shifted to match those of the earlier coronal wave front peak(s). We present our interpretation of this phase shift in § 3.1.

2.2. *Radial Features of the Coronal Waves*

Intensity profiles (Fig. 3) made in a radial direction from the center of the disturbance reveal the diffuse brightening to be consistently concentrated in two places; at the outermost edge of the deep dimming regions and simultaneously at the leading edge of the expanding wave front. The brightenings show an increase in intensity by a factor of 8 (May 12) and factor of 6 (April 7) of the respective quiet-Sun intensities.

The base difference images in Figure 3 also show widespread

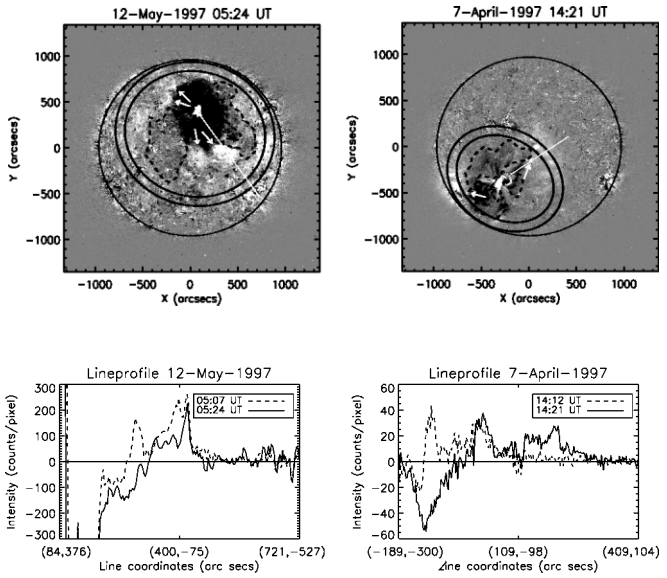

FIG. 3.—Top panels show the later base difference image for the May 12 (*left*) and April 7 (*right*) events, with the fitted black ellipses (Fig. 1) marking the location of the expanded coronal wave front. Concentrations of intensity are located at the edge of the deep core dimming regions (*white arrows*) and simultaneously at the leading edge of the coronal wave in both cases. The black dashed lines enclose regions of widespread diffuse dimming. The lower panels show intensity profiles made along the straight white lines in the top panels. The dashed (solid) lines show the intensity profiles from the earlier (later) base difference heliograms.

diffuse dimmings associated with each event (*regions bounded by black dashed lines*), and persistent brightenings are marked by white arrows at the edge of the deep dimmings. In contrast to the deep core dimmings seen in the intensity profiles of Figure 3 (also see Attrill et al. 2006; Zarro et al. 1999), the diffuse dimmings are weak and extend to large distances from the core dimmings. They rapidly propagate across the solar disk, behind the leading bright front.

3. INTERPRETATION

3.1. *Phase Shift of Intensity as a Function of Azimuthal Angle*

Figure 2 shows a phase shift of the mean intensity for each event, being 44° counterclockwise (CCW) for the May 12 peak (confirming the result obtained by Podladchikova & Berghmans 2005) and 22° clockwise (CW) for both peaks of the April 7 event.

From the standard flare model (e.g., Shibata et al. 1995) the erupting filament/flux rope forms the core of the CME and is the driver of the "skirt" of the CME. If this skirt corresponds to the coronal wave front, then one expects the behavior of the coronal wave to be linked with that of the filament. Webb et al. (2000) describe a CCW rotation of the partially erupting filament, just prior to the coronal wave event on May 12. We therefore interpret the phase shift of the EIT bright front (Fig. 2) as an indication that the rotation of the CME magnetic structure continued following the initial rotation of the erupting core. Although a CW rotation is suggested for the April 7 case (Green et al. 2007), it is more difficult to confidently analyze the Hα data because projection effects become important. In addition, the source region helicity is different for each event (§ 2.1).

If the helicity of the source region determines the sense of the subsequent rotation of the coronal wave front (identified above as the skirt of the CME), then this poses a challenge to the standard MHD "blast wave" interpretation: why should a flare-induced blast wave take account of the helicity of the CME source region? Our results suggest that the EIT coronal wave is driven by the erupting magnetic configuration, rather than by a blast wave.

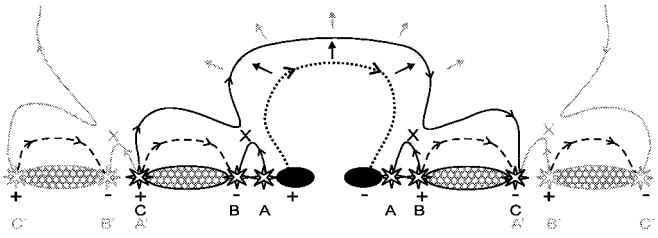

FIG. 4.—Cartoon illustrating the magnetic reconnection model proposed to generate the bright, diffuse coronal "wave" front, with the observed dual brightenings and two types of dimmings. The expanding CME (*dotted line*) reconnects with favourably orientated quiet-Sun magnetic loops (*dashed lines*), displacing the footpoints of the expanding CME (*solid line*). The crosses mark regions where magnetic reconnection occurs. The dotted/dashed lines show the pre-eruption magnetic structures, the black (gray) solid lines show the result of the first (subsequent) reconnections.

3.2. *Our Model*

We therefore propose a new mechanism where the bright fronts that constitute the diffuse EIT "wave front" are due to heating caused by the expanding CME magnetic field being thrust into and reconnecting with favorably orientated "open" or "closed" magnetic structures. Since the two events we analyze occurred in a quiet-Sun (QS) environment, we focus here on interaction with QS loops and scattered "open" field lines.

With reference to Figure 4, the expanding CME structure (*dotted line*) reconnects with surrounding favorably orientated QS loops (*dashed lines*). These reconnections produce brightenings at points A, B, and C, as a result of chromospheric evaporation (this is a lower energy version of the physics that happens in flares). The flux rope is assumed to expand in all directions at about the same rate and to be anchored in the deep dimming regions. It is the low part of the flux rope (near the footpoints) that is able to reconnect the most with low-lying QS loops, hence the concentrations in intensity (Fig. 2). Brightenings A may be mixed with the deep dimming or be spatially unresolvable from brightenings B, thus forming the brightening at the edge of the deep dimmings, while brightenings C are responsible for the leading edge bright wave front. Together, these brightenings make up the diffuse dual-brightening coronal wave (Fig. 3).

The brightening from each reconnected loop will progressively disappear on the timescale defined by the thermal cooling of the plasma. However, an almost stationary brightening located at the edge of the deep dimmings (*black regions*) persists (Fig. 3), because the expanding core magnetic structure continues to drive reconnections with the low-lying loops there.

The reconnection can also create longer field lines (Fig. 4, *solid lines*) and therefore a larger volume within the expanding CME cavity (brightenings C are displaced CME footpoints). Plasma previously contained by the closed QS loops (*dashed lines*) is suddenly released into a much larger volume. As a result, we observe diffuse dimming (*hatched regions*) that can develop only after the brightenings have occurred. Reconnection with "open" field lines would only create brightenings A and B and would not contribute to the appearance of the diffuse dimmings. Given the large spatial distribution of the diffuse dimmings for these events (Fig. 3), we believe that reconnection with QS loops is a more important process in the studied two cases.

After the first reconnections, the continuing expansion drives

the dual-brightening signatures of the subsequent reconnections. The diffuse leading edge bright front therefore appears to propagate, being formed by successive reconnections with QS loops progressively farther away, forming many brightenings A', B', and C'. This implies a progression of the diffuse "EIT wave" front by steps, with a global average motion defined by the expansion of the CME core. Our model does not require a preexisting giant bipolar arcade to span the diameter of the observed coronal wave (as in Chen et al. 2002), since this is naturally created by the displacement of the expanding CME footpoints, through the successive small-scale reconnection events between the erupting magnetic configuration and QS loops. This new model thus provides a natural mechanism via which CMEs can become large-scale in the lower corona.

4. CONCLUSIONS

The behavior of the diffuse coronal bright front appears to be linked to the helicity of the source region and to the sense of rotation of the erupting flux rope/filament. The apparently discerning rotation of the bright fronts poses an interesting challenge to the interpretation of these phenomena as flare induced blast waves.

We propose that the diffuse EIT coronal bright fronts are due to driven magnetic reconnections between the skirt of the expanding CME magnetic field and favorably orientated QS magnetic loops. Such a mechanism appears to explain the dual bright fronts and the widespread diffuse dimming, while the deep dimmings correspond to the expansion of the core footpoints of the erupting flux rope.

With the above model, we suggest that diffuse EIT bright fronts do not "stop" at or "avoid" active regions or coronal holes (Thompson et al. 1998, 1999). Rather, they slow down substantially, and they undergo many magnetic reconnections if the skirt of the CME encounters a concentrated region of favorably orientated magnetic field. Or conversely, if the skirt encounters a region of unfavorably orientated magnetic field, then the conditions required for magnetic reconnection will not exist, and the bright front will vanish.

The higher time cadence of data from *Hinode*, the *Solar Terrestrial Relations Observatory*, and the *Solar Dynamics Observatory* should allow a greater statistical analysis of the relationship between the helicity of the event source region, the sense of rotation of the erupting filament/flux rope, and the behavior displayed by the expanding coronal bright front.

We thank the referee for helpful comments and I. V. Alexeev for useful discussions. G. D. R. A. is grateful to PPARC for support. L. K. H. acknowledges the Leverhulme Trust for the award of a Philip Leverhulme prize. L. V. D.-G. acknowledges the Hungarian government grant OTKA T048961.

REFERENCES

Attrill, G., Nakwacki, N., Harra, L. K., van Driel-Gesztelyi, L., Mandrini, C. H., Dasso, S., & Wang, J. 2006, Sol. Phys., 238, 117
Aurass, H., Vršnak, B., & Mann, G. 2002, A&A, 384, 273
Balasubramaniam, K. S., Pevtsov, A. A., Neidig, D. F., Cliver, E. W., Thompson, B. J., Young, C. A., Martin, S. F., & Kiplinger, A. 2005, ApJ, 630, 1160
Ballai, I., Erdélyi, R., & Pintér, B. 2005, ApJ, 633, L145
Biesecker, D. A., Myers, D. C., Thompson, B. J., Hammer, D. M., & Vourlidas, A. 2002, ApJ, 569, 1009
Chen, P. F. 2006, ApJ, 641, L153
Chen, P. F., Wu, S. T., Shibata, K., & Fang, C. 2002, ApJ, 572, L99
Chertok, I. M., & Grechnev, V. V. 2005, Sol. Phys., 229, 95
Cliver, E. W., Laurenza, M., Storini, M., & Thompson, B. J. 2005, ApJ, 631, 604
Cliver, E. W., Nitta, N. V., Thompson, B. J., & Zhang, J. 2004, Sol. Phys., 225, 105
DeForest, C. E. 2004, Sol. Phys., 219, 3
Delaboudinière, J. P., et al. 1995, Sol. Phys., 162, 291
Delannée, C. 2000, ApJ, 545, 512
Delannée, C., & Aulanier, G. 1999, Sol. Phys., 190, 107
Green, L. M., Kliem, B., Török, T., van Driel-Gesztelyi, L., & Attrill, G. 2007, Sol. Phys., submitted
Harra, L. K., & Sterling, A. C. 2003, ApJ, 587, 429
Khan, J. I., & Aurass, H. 2002, A&A, 383, 1018
Klassen, A., Aurass, H., Mann, G., & Thompson, B. J. 2000, A&AS, 141, 357
Leamon, R. J., Canfield, R. C., & Pevtsov, A. A. 2002, J. Geophys. Res., 107, 1234
Manoharan, P. K., van Driel-Gesztelyi, L., Pick, M., & Démoulin, P. 1996, ApJ, 468, L73
Moreton, G. E. 1960, AJ, 65, 494
Ofman, L., & Thompson, B. J. 2002, ApJ, 574, 440
Podladchikova, O., & Berghmans, D. 2005, Sol. Phys., 228, 265
Shibata, K., Masuda, S., Shimojo, M., Hara, H., Yokoyama, T., Tsuneta, S., Kosugi, T., & Ogawara, Y. 1995, ApJ, 451, L83
Thompson, B. J., Cliver, E. W., Nitta, N., Delannée, C., & Delaboudinière, J. P. 2000a, Geophys. Res. Lett., 27, 1431
Thompson, B. J., Plunkett, S. P., Gurman, J. B., Newmark, J. S., St. Cyr, O. C., & Michels, D. J. 1998, Geophys. Res. Lett., 25, 2461
Thompson, B. J., Reynolds, B., Aurass, H., Gopalswamy, N., Gurman, J. B., Hudson, H. S., Martin, S. F., & St. Cyr, O. C. 2000b, Sol. Phys., 193, 161
Thompson, B. J., et al. 1999, ApJ, 517, L151
Uchida, Y. 1968, Sol. Phys., 4, 30
Wang, Y. M. 2000, ApJ, 543, L89
Warmuth, A., Vršnak, B., Aurass, H., & Hanslmeier, A. 2001, ApJ, 560, L105
Warmuth, A., Vršnak, B., Magdalenic, J., Hanslmeier, A., & Otruba, W. 2004a, A&A, 418, 1101
———. 2004b, A&A, 418, 1117
Webb, D. F., Lepping, R. P., Burlaga, L. F., DeForest, C. E., Larson, D. E., Martin, S. F., Plunkett, S. P., & Rust, D. M. 2000, J. Geophys. Res., 105, 27251
Zarro, D. M., Sterling, A. C., Thompson, B. J., Hudson, H. S., & Nitta, N. 1999, ApJ, 520, L139
Zhukov, A. N., & Auchère, F. 2004, A&A, 427, 705